Observations of second baroclinic mode internal solitary waves on the continental slope of the northern South China Sea

Yiing Jang Yang,[1] Ying Chih Fang,[2] Ming-Huei Chang,[2,3] Steven R. Ramp,[4,5] Chih-Chung Kao,[6] and Tswen Yung Tang[2]

Received 8 February 2009; revised 9 July 2009; accepted 16 July 2009; published 3 October 2009.

[1] A temperature and current velocity mooring, located on the upper continental slope of the northern South China Sea, recorded a number of second baroclinic mode (mode 2) internal solitary waves (ISWs). These types of waves are seldom observed in nature. The mode 2 ISWs typically showed upward (downward) displacement of isotherms in the upper (lower) water column and three layers of eastward, westward, and eastward current from the uppermost to bottommost portions of a wave. In summer, westward-propagating mode 2 ISWs were observed only occasionally. These waves generally appeared after mode 1 ISWs, a feature that may relate to the diurnal tide with a period of approximately 24 hours. The displacement of isotherms induced by mode 2 ISWs was 20 ± 14 m at 75 m and −22 ± 15 m at 240 m, and the characteristic time scale was approximately 8.0 ± 4.3 min. In winter, mode 2 ISWs were more active but mode 1 ISWs were rarely observed. Isotherm displacement by mode 2 ISWs in winter was 30 ± 18 m at 75 m and −26 ± 16 m at 240 m, and the average characteristic time scale was 6.9 ± 4.6 min. The mode 2 ISWs thus had larger amplitudes and smaller time scales in winter than they did in summer. The observed vertical temperature profile also showed notable seasonal change. The thermocline was shallow in summer and deep in winter. In winter, vertical temperature profiles indicated that the main thermocline was located near middepth over the upper continental slope near the 350 m isobath. Mode 1 ISWs were more active in summer than in winter, reflecting the larger Ursell numbers for mode 1 ISWs in summer. Among mode 2 ISWs in summer, 90% appeared after mode 1 ISWs. These results suggest that mode 2 ISWs could be related to mode 1 ISWs. In contrast, mode 2 ISWs were more active in winter than in summer, with larger mode 2 Ursell numbers also found in winter. Among winter mode 2 ISWs, 72% appeared without mode 1 ISWs. Mode 2 ISWs in winter could be related to the main thermocline being located near middepth. These seasonal variations of mode 2 ISWs were correlated with the seasonal change of local stratification. Further study on the different generating mechanisms of mode 2 ISWs in summer and winter is needed.

Citation: Yang, Y. J., Y. C. Fang, M.-H. Chang, S. R. Ramp, C.-C. Kao, and T. Y. Tang (2009), Observations of second baroclinic mode internal solitary waves on the continental slope of the northern South China Sea, *J. Geophys. Res.*, *114*, C10003, doi:10.1029/2009JC005318.

1. Introduction

[2] An internal solitary wave (ISW) is a localized internal gravity wave that occurs in a stratified ocean. These waves greatly impact the ocean environment as well as offshore engineering. For example, ISWs produce strong vertical motions that induce nutrient pumping [*Sandstrom and Elliott*, 1984] and sediment resuspension [*Bogucki et al.*, 2005; *Boegman and Ivey*, 2009; *Stastna and Lamp*, 2008]. The large vertical shear produced by the horizontal velocity of these waves also presents a hazard to oil platforms [*Bole et al.*, 1994]. Most observed ISWs can be categorized as first baroclinic mode waves (hereafter referred to as mode 1 ISWs). A mode 1 ISW displaces isotherms downward in deep water, but upward if the upper layer becomes thicker than the lower layer. The former is known as a depression wave, and the latter is known as an elevation wave. Recent review papers by *Helfrich and Melville* [2006] and *Apel et al.* [2007] describe theoretical and observational studies of mode 1 ISWs.

[1]Department of Marine Science, Naval Academy, Kaohsiung, Taiwan.
[2]Institute of Oceanography, National Taiwan University, Taipei, Taiwan.
[3]Now at Department of Marine Environmental Informatics, National Taiwan Ocean University, Keelung, Taiwan.
[4]Department of Oceanography, Naval Postgraduate School, Monterey, California, USA.
[5]Now at Monterey Bay Aquarium Research Institute, Moss Landing, California, USA.
[6]Department of Information Management, Fortune Institute of Technology, Kaohsiung, Taiwan.

0148-0227/09/2009JC005318

[3] However, while mode 1 ISWs have been extensively investigated, the second baroclinic mode wave (hereafter referred to as mode 2 ISW) has received less research attention and few observational studies have documented this wave type. Laboratory experiments first revealed the properties of the mode 2 ISW. *Davis and Acrivos* [1967] generated mode 2 ISWs in a three-layer water tank with an initial condition consisting of a thin middle layer of uneven density lying between layers of constant density. After introducing some mixed fluid into the middle layer, the upper interface (between the surface and middle layer) and the lower interface (between the bottom and the middle) were displaced upward and downward, respectively, producing the ''double-hump'' waveform characteristic of a mode 2 ISW. Such a wave can propagate along the middle layer of a three-layer fluid for a long distance. *Benjamin* [1967] derived a weakly nonlinear analytic solution for the small-amplitude mode 2 ISW using an inviscid stream function equation by assuming a hyperbolic tangent density profile. The solution showed that a solitary wave propagated along the thin middle layer with uneven density in an unbounded fluid. Above the middle layer, an elevation wave was obtained, while below the middle layer, a depression wave was obtained [*Benjamin*, 1967]. The analytic solution of the mode 2 ISW thus had a symmetric ''bulge'' shape about the middle layer. The analytical solution was limited by a symmetric density distribution around some depth [*Tung et al.*, 1982].

[4] Recent mode 2 ISW studies have included theoretical investigations [*Benjamin*, 1967; *Davis and Acrivos*, 1967; *Akylas and Grimshaw*, 1992; *Vlasenko*, 1994], laboratory experiments [*Davis and Acrivos*, 1967; *Maxworthy*, 1980; *Kao and Pao*, 1980; *Honji et al.*, 1995; *Stamp and Jacka*, 1995; *Vlasenko and Hutter*, 2001; *Mehta et al.*, 2002; *Sutherland*, 2002], and numerical analyses [*Tung et al.*, 1982; *Terez and Knio*, 1998; *Rubino et al.*, 2001; *Vlasenko and Hutter*, 2001; *Rusås and Grue*, 2002; *Stastna and Peltier*, 2005; *Vlasenko and Alpers*, 2005]. Most studies have concentrated on the generation, existence, and form of mode 2 ISWs and have presented five potential generation mechanisms for the waves: a mode 1 ISW propagating onshore and entering the breaking instability stage [*Helfrich and Melville*, 1986]; a mode 1 ISW flowing over a sill [*Konyaev et al.*, 1995; *Vlasenko and Hutter*, 2001]; intrusion of the whole head of a gravity current into a three-layer fluid [*Mehta et al.*, 2002]; flow over negative topography under a background condition of the main thermocline located near middepth [*Stastna and Peltier*, 2005]; and reflection of a mode 1 ISW [*Chao et al.*, 2006].

[5] Mode 2 ISWs have been observed at only a few locations in the world, such as Knight Inlet on the coast of British Columbia [*Farmer and Smith*, 1980], Mascarene Ridge in the Indian Ocean [*Konyaev et al.*, 1995; *Sabinin and Serebryany*, 2005], the New Jersey shelf [*Moum et al.*, 2008], the continental shelf in the northern South China Sea [*Duda et al.*, 2004; *Yang et al.*, 2004], and lakes Biwa (Japan) and Kinneret (Israel) [*Saggio and Imberger*, 1998, 2001; *Antenucci et al.*, 2000; *Boegman et al.*, 2003]. Each of those field programs was relatively short and recorded only a few mode 2 ISWs, not enough to compute wave statistics.

[6] In the northern South China Sea, mode 1 ISWs are common (see Figure 1) [*Kao et al.*, 2006, 2007] and the largest waves of this type in the world have been recorded [*Ramp et al.*, 2004]. Mode 1 depression ISWs may evolve primarily from the internal tide that is generated around the Luzon Strait and propagates to the west [*Lien et al.*, 2005; *Chao et al.*, 2007; *Helfrich and Grimshaw*, 2008; *Shaw et al.*, 2009]. This type of wave may form around the continental shelf east of Dongsha Atoll [*Ramp et al.*, 2004]. Mode 2 ISWs are also often found in the northern South China Sea. However, mode 2 waves have attracted little attention. During the Asian Seas International Acoustics Experiment (ASIAEX) [*Ramp et al.*, 2003; *Lynch et al.*, 2004], mode 2 ISWs were observed at moorings IW1, IW3, S4, S5, and S7 over the continental slope of the northern South China Sea (Figure 1) [*Yang et al.*, 2000, 2004; *Duda et al.*, 2004]. Table 1 summarizes previous measurements of mode 2 ISWs on the continental slope/shelf of the northern South China Sea. Mode 2 ISWs appeared during neap and spring tides and generally, but not always, followed mode 1 ISWs. The characteristics of mode 2 ISWs were unclear. Fortunately, in 2005 and 2006, a long-term mooring array was deployed from the Luzon Strait to the shelf of the northern South China Sea (Figure 1) under the joint research program known as Variations Around the Northern South China Sea (VANS; supported by Taiwan) and the Windy Islands Soliton Experiment (WISE; supported by the United States). The moored current meters and temperature sensors at mooring S7 on the continental slope (Figure 1) recorded many mode 2 ISWs. This paper describes the characteristics of these mode 2 ISWs on the continental slope of the northern South China Sea and discusses their seasonal variation.

[7] The remainder of this paper is organized as follows. Section 2 describes the fieldwork and measurement results, presenting two segments of observations during summer and winter. Section 3 gives analysis results for mode 2 ISWs, including their vertical structure, amplitude, characteristic scale, and the environmental parameters of the Korteweg-de Vries (K-dV) equation. Finally, section 4 provides a discussion and a summary.

2. Measurement

2.1. Fieldwork

[8] Under the Taiwan/U.S. joint research program VANS/WISE, several moorings were deployed across the continental slope of the northern South China Sea (Figure 1). Unfortunately, two of the shelf moorings were lost due to fishing activities in the shelf area. The continental slope mooring, S7, successfully recorded a number of mode 2 ISW episodes. No mode 2 ISWs were recorded by moorings in deep basin (Figure 1). Thus, we use only data from mooring S7 to describe the characteristics and seasonal variations of mode 2 ISWs on the continental slope of the northern South China Sea. Mooring S7 was deployed at 350 m depth from 29 April to 28 July 2005 and from 2 November 2005 to 24 February 2006 (Figure 1). It included one acoustic Doppler current profiler (ADCP), three ducted paddlewheel recording current meters (RCM8s), seven temperature-pressure recorders (TPs), four conductivity-temperature-depth (CTD) sensors, and one temperature recorder (T-pod). The 300 kHz broadband self-contained ADCP was moored at 100 m depth looking upward and provided current information from 15 to 95 m in 4 m bins.

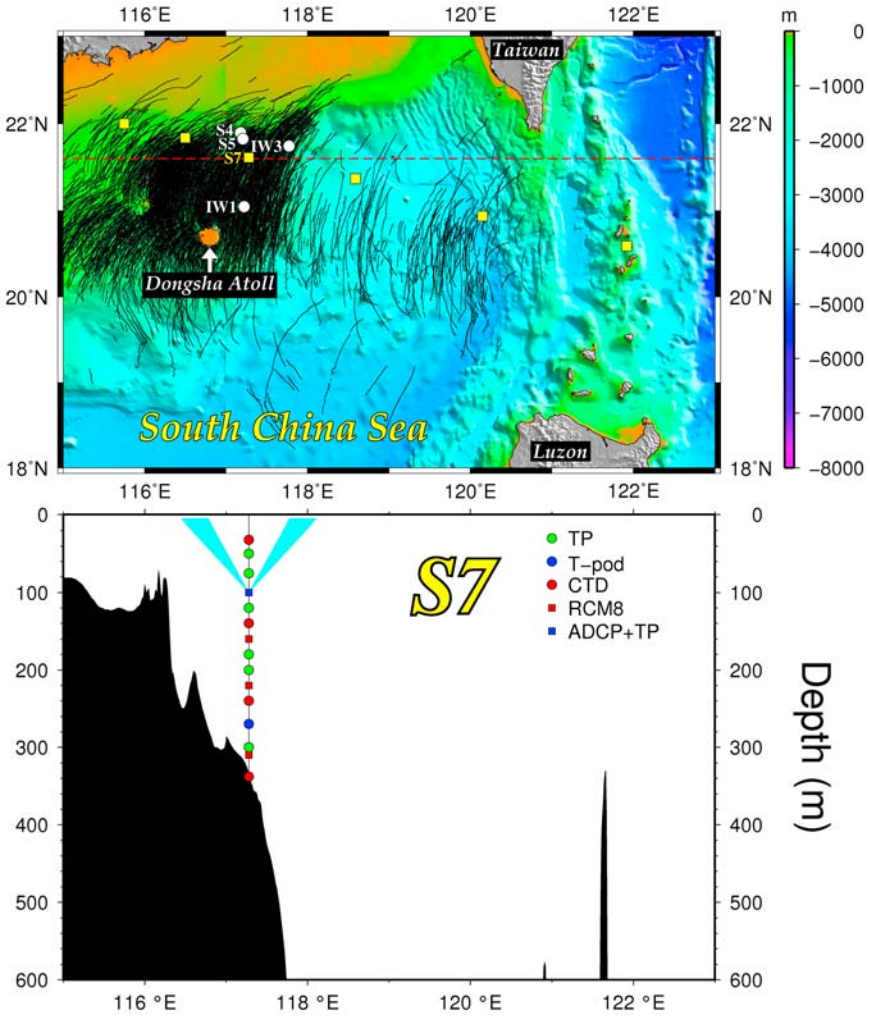

Figure 1. (top) Map showing the distribution of ISWs observed in 348 MODIS images acquired from the Terra and Aqua satellites between 2002 and 2007 in the northern South China Sea [from *Kao et al.*, 2006, 2007]. The white solid circle and yellow solid squares represent the locations of the ASIAEX and VANS/WISE moorings, respectively. (bottom) The bottom topography along 21.6°N (red dashed line in Figure 1 (top)) with a diagram showing the position and instrument locations on mooring S7.

The ADCP ping rate was 1 s, and the averaging interval was 1 min. Beneath the ADCP, three RCM8s were mounted at 160, 220, and 310 m. The RCM8s recorded the current velocity every 5 min. The TPs and T-pod sampled every 1 min and the CTDs sampled every 2 min from 32 to 338 m. Table 2 summarizes the data return for all the moored instruments. The first and second measurement periods represent the summer and winter seasons, respectively.

Table 1. Summary of Previous Measurements of Second Baroclinic Mode Internal Solitary Waves on the Continental Slope/Shelf of the Northern South China Sea

Mooring	Location		Local Depth (m)	Emergence Time (UT)	Spring/Neap Tide	Leading Mode 1 ISW
	Latitude	Longitude				
IW1	21° 3.38′N	117° 12.60′E	426	10 Apr 1999 0230	Neap	No
IW3	21° 44.53′N	117° 46.31′E	468	7 Apr 2000 1928	Spring	Yes
	21° 44.53′N	117° 46.31′E	468	8 Apr 2000 1430	Spring	Yes
S4	21° 53.94′N	117° 10.62′E	120	22 Apr 2001 0728	Spring	Yes
	21° 53.94′N	117° 10.62′E	120	23 Apr 2001 1216	Spring	Yes
	21° 53.94′N	117° 10.62′E	120	5 May 2001 1210	Spring	Yes
	21° 53.94′N	117° 10.62′E	120	6 May 2001 1330	Spring	Yes
S5	21° 49.35′N	117° 12.33′E	202	22 Apr 2001 0215	Spring	Yes
S7	21° 36.87′N	117° 16.98′E	350	1 May 2001 0055	Neap	Yes
	21° 36.87′N	117° 16.98′E	350	2 May 2001 0528	Neap	Yes
	21° 36.87′N	117° 16.98′E	350	2 May 2001 0952	Neap	Yes
	21° 36.87′N	117° 16.98′E	350	6 May 2001 0223	Spring	Yes

Table 2. Summary of the Mooring Information

Instrument Depth (m)	Instrument	Period I	Period II	Sampling Rate (min)
32	CTD	29 Apr 2005 to 21 Jul 2005	2 Nov 2005 to 24 Feb 2006	2
50	TP	29 Apr 2005 to 21 Jul 2005	2 Nov 2005 to 24 Feb 2006	1
75	TP	29 Apr 2005 to 21 Jul 2005	2 Nov 2005 to 24 Feb 2006	1
100	TP	29 Apr 2005 to 21 Jul 2005	2 Nov 2005 to 24 Feb 2006	1
100[a]	ADCP	29 Apr 2005 to 21 Jul 2005	2 Nov 2005 to 18 Jan 2006	1
120	TP	29 Apr 2005 to 21 Jul 2005	2 Nov 2005 to 24 Feb 2006	1
140	CTD	29 Apr 2005 to 21 Jul 2005	2 Nov 2005 to 24 Feb 2006	2
160	RCM8	29 Apr 2005 to 21 Jul 2005	2 Nov 2005 to 21 Feb 2006	5
180	TP	29 Apr 2005 to 21 Jul 2005	2 Nov 2005 to 24 Feb 2006	1
200	TP	29 Apr 2005 to 21 Jul 2005	2 Nov 2005 to 24 Feb 2006	1
220	RCM8	29 Apr 2005 to 21 Jul 2005	2 Nov 2005 to 21 Feb 2006	5
240	CTD	29 Apr 2005 to 21 Jul 2005	2 Nov 2005 to 24 Feb 2006	2
270	T-pod	29 Apr 2005 to 21 Jul 2005	2 Nov 2005 to 24 Feb 2006	1
300	TP	29 Apr 2005 to 21 Jul 2005	2 Nov 2005 to 24 Feb 2006	1
310	RCM8	29 Apr 2005 to 21 Jul 2005	2 Nov 2005 to 21 Feb 2006	5
338	CTD	29 Apr 2005 to 21 Jul 2005	2 Nov 2005 to 24 Feb 2006	2

[a]Bin length is 4 and range is 15∼95.

[9] Figure 2 shows an example of a mode 2 ISW, which passed the mooring site around 2340 UT on 27 June 2005. When the wave passed the mooring location, the temperature profile data showed decreasing and then increasing temperature in the upper layer and the opposite temperature pattern in the lower layer. Therefore, a mode 2 ISW episode can be easily identified from the time series of temperature profile data. In this paper, we use this thermal displacement pattern to define a mode 2 ISW. The nodal point of vertical motion was between 100 and 160 m. Eastward current component (u) data showed eastward acceleration and then deceleration above 60 m and at 220 and 310 m, and the opposite pattern between 60 and 100 m and at 160 m. There were two nodal points of u: an upper point around 60 m and a lower one between 160 and 220 m (Figure 2 (middle)). The northward current component (v) variations induced by the mode 2 ISW were the same as u, whereas the amplitude of v was smaller than that of u. The mode 2 ISW propagation direction was consistent with the current direction in the middle layer. Therefore, the primary propagation direction of this mode 2 ISW was westward.

2.2. Observations in Summer

[10] Twenty episodes of mode 2 ISWs were identified in summer. Figure 3 shows temperature contour plots as a function of depth and time from 24 to 27 June 2005. Previous studies have suggested that a mode 2 ISW can evolve from a mode 1 ISW undergoing a shoaling process [*Helfrich and Melville*, 1986]. Therefore, we examined the time series data to see whether a leading mode 1 ISW occurred ahead of the mode 2 episodes. As observed in Figure 3, one to two mode 1 depression ISW packets passed the mooring each

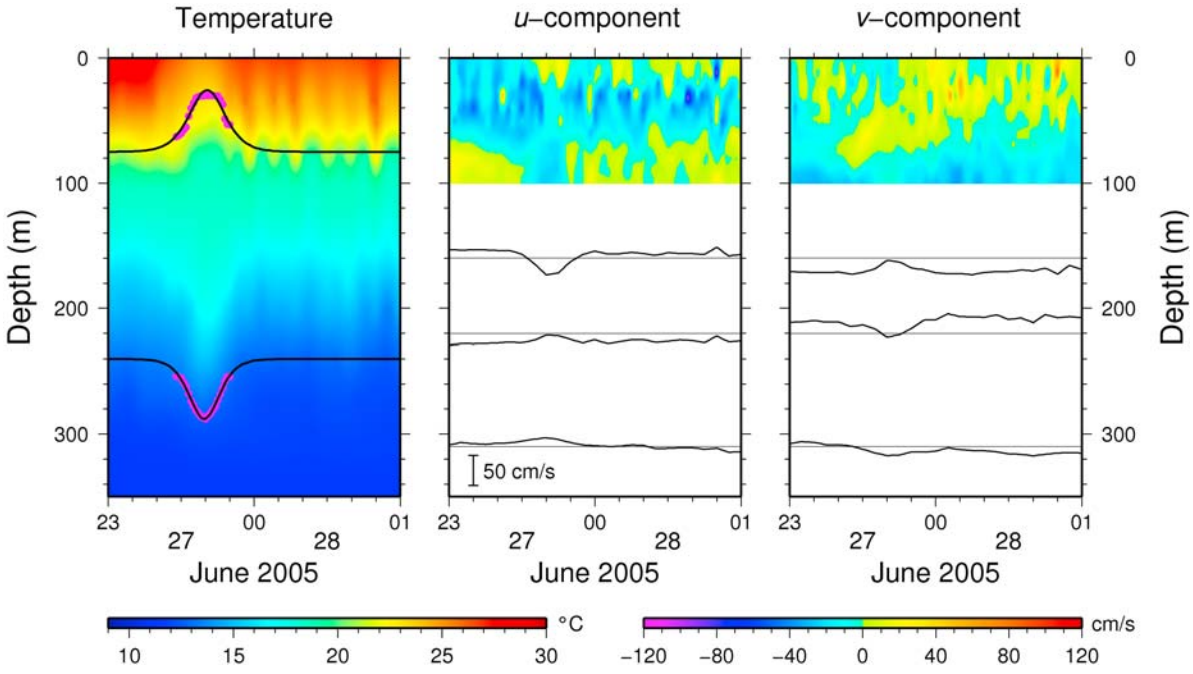

Figure 2. The (left) temperature, (middle) u component, and (right) v component from 2300 UT on 27 June 2005 to 0100 UT on 28 June 2005. Figure 2 (left) also displays the isothermal displacement (solid purple circles) and the fitted curve obtained by using a squared hyperbolic secant function at 75 and 240 m (solid lines). The current data were measured by an ADCP between 15 and 95 m and three RCM8s at 160, 220, and 310 m.

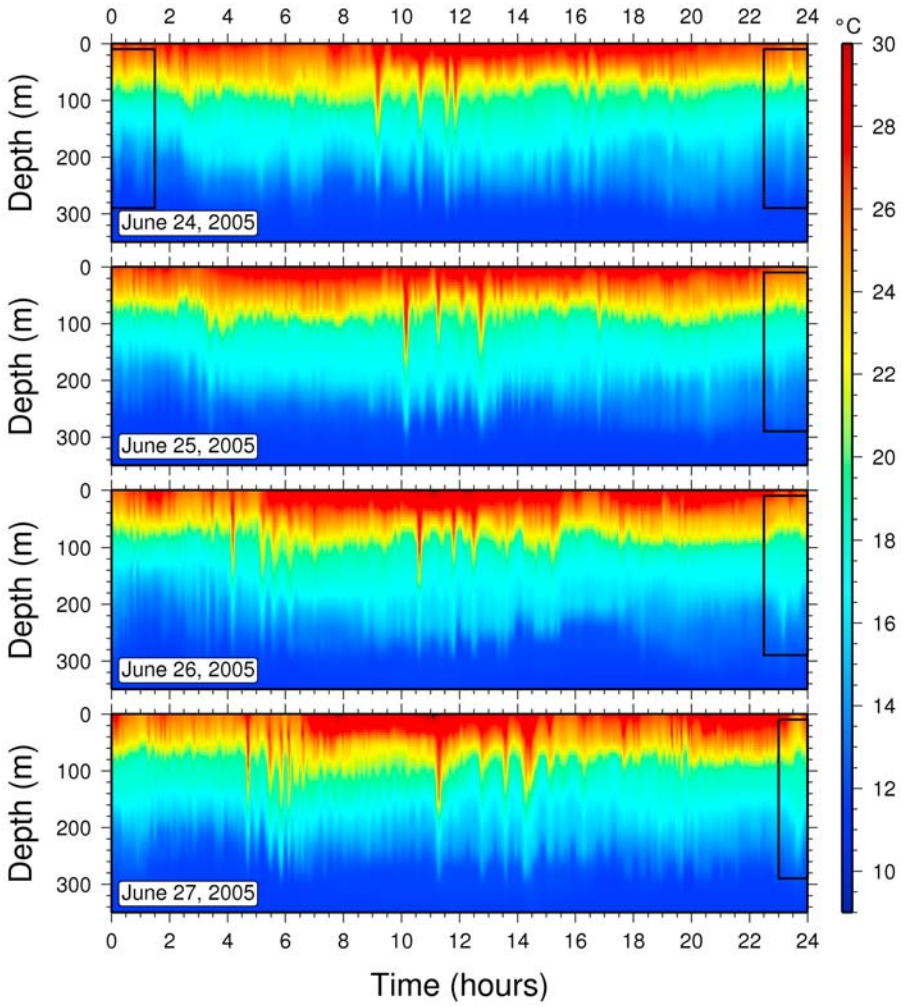

Figure 3. Color contours of isotherm depth from 24 June to 27 June 2005. The black rectangle indicates the mode 2 ISW.

day. These results are consistent with those of *Ramp et al.* [2004], who showed that two types of mode 1 depression ISW packets arrived in this area. One type appeared regularly every 24 hours and was thought to be related to the K_1 tide. The other arrived about 1 hour later every day and was possibly related to the M_2 tide [*Ramp et al.*, 2004]. In this case during June 2005 (Figure 3), both the stronger packets (arriving at 0914, 1012, 1040, and 1122 UT on 24–27 June, respectively) and the weaker packets (arriving at 0250, 0326, 0416, and 0446 UT) arrived a little later each day. However, using the data from the months before and after, and from deep basin mooring (not shown) it can be shown that the stronger packets arriving later in the day were the diurnal (type a) waves and the weaker packets arriving earlier in the day were the semidiurnal (type b) waves. The mode 2 waves (highlighted by the black rectangles in Figure 3) arrived in their own unique time slot approximately 12.5 hours after the leading type a wave, between 2300 and 2400 UT each day. Since the mode 2 waves were not observed in the deep basin, this suggests that the generation of the mode 2 waves may be related to the large type a wave packets interacting with the continental slope in summer. This idea is discussed later in more detail.

[11] Five mode 2 ISW packets are highlighted by black rectangles in Figure 3; the emergence of these packets was later than mode 1 ISW packets by about 12 hours. Another notable finding was that one mode 2 ISW emerged each day at around 2330 UT from 24 to 27 June. A mode 2 ISW appeared around 0000 UT on 24 June. The late appearance of the wave could have been due to slower phase speed or later generation time. The mode 2 ISWs appeared regularly, arriving at the mooring site about every 24 hours. Accordingly, these mode 2 ISWs could have been related to the diurnal internal tide interacting with the continental slope. In addition, numerous studies have suggested that the existence of a mode 1 ISW could also be important for mode 2 ISWs. This is discussed later in detail.

[12] In this study, the current at 160 m depth was used to determine the propagation direction of the mode 2 ISW. We selected current data at times midway through mode 2 ISW passage by the mooring, with the background current removed. The background current was defined as the current averaged over the 30 min before the arrival of the wave. The rose diagram in Figure 4 shows the summer distribution of wave speed and direction for 20 episodes of mode 2 ISW passage. These diagrams show that most of the mode 2 ISWs propagated westward.

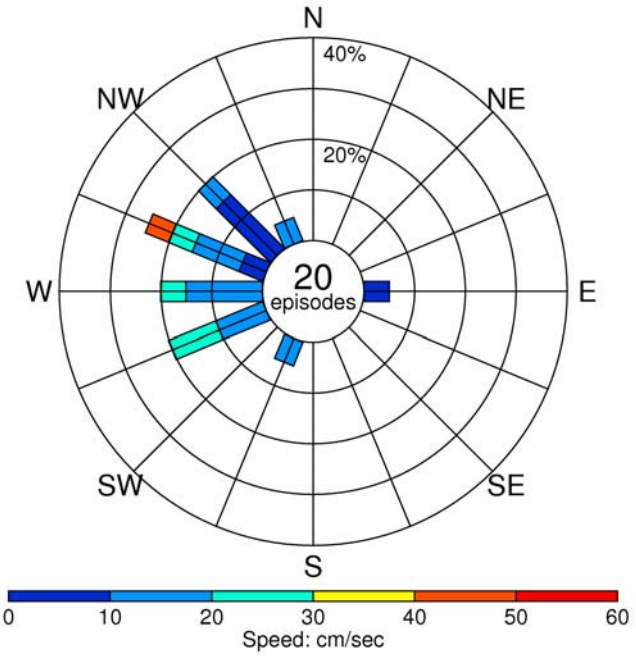

Figure 4. Histogram of mode 2 wave speed and direction at 160 m in summer. The length of each bar is proportional to the percentage of times when that current speed (and below) was observed toward that direction. The data were high-pass filtered to remove the background currents. Different colors on each bar indicate the current speed.

2.3. Observations in Winter

[13] Fifty-eight episodes of mode 2 ISWs were observed in winter. Figure 5 is similar to Figure 3 but for observations in winter from 24 to 27 December 2005. Each black rectangle highlights a mode 2 ISW packet. Figure 5 shows that the situation in winter differed from that in summer. No apparent mode 1 depression ISW was found, although several short-wavelength elevation waves emerged behind the mode 2 ISW. This result agrees with the findings of *Shaw et al.* [2009], who concluded that the deeper mixed layer in winter suppresses the production of mode 1 ISWs. Eight mode 2 ISW packets were observed in 4 days, some with two or three consecutive waves. The most remarkable feature is that mode 2 ISWs appeared randomly but frequently. Unlike mode 2 ISWs related to tidal forcing in summer, the random appearance of mode 2 ISWs in winter indicates that these waves were perhaps unrelated to tidal forcing. The seasonal difference will be discussed later in this paper.

[14] Figure 6 presents an example of a mode 2 ISW in winter. This mode 2 ISW passed the S7 mooring site at around 1052 UT on 27 December 2005. The nodal point of the temperature fluctuation was around 150 m, which was deeper than the summer case. The horizontal current variations were smaller than in the summer case. The nodal points of horizontal velocity were around 80 m and below 220 m, deeper than those found in the summer case. Furthermore, the time scale of the winter case was also smaller than that in the summer case. The rose diagram in Figure 7 shows the statistical results from 58 mode 2 ISW events in winter. The most common direction was westward, but the distribution was more uniform, indicating possible local generation.

3. Analysis

3.1. Modal Functions

3.1.1. Theory

[15] Hydrostatic, frictionless internal motion with no background current satisfies the Boussinesq approximation, and the vertical structure functions of displacement or motion W_n are governed by the Taylor-Goldstein equation [*Gill*, 1982]

$$\frac{d^2W_n(z)}{dz^2} + \frac{N^2(z)}{c_n^2}W_n(z) = 0, \tag{1}$$

subject to rigid lid boundary conditions, where $W_n(z)$ is the eigenfunction (or vertical structure function) for the nth mode, c_n is the eigenvalue (or linear wave phase speed), and $N(z)$ is the Brunt-Väisälä (or buoyancy) frequency. The vertical modes of horizontal $U_n(z)$ and vertical motion are related by $U_n(z) = dW_n(z)/dz$. The theoretical vertical structures can be calculated using the buoyancy frequency profile. The buoyancy frequency was calculated using 36 hour low-pass-filtered temperature profile time series data and assuming a constant salinity of 35.0 practical salinity unit.

[16] According to *Lee and Beardsley* [1974], *Apel et al.* [1997], and *Apel* [2003], the modal expansion of the fundamental hydrodynamics equations, neglecting rotational effects and energy exchange between modes, and assuming weakly nonlinear finite amplitude plane progressive waves propagating in a specific direction, the modal displacement η_n governed by the K-dV equation [*Korteweg and deVries*, 1895] is

$$\frac{\partial\eta_n}{\partial t} + c_n\frac{\partial\eta_n}{\partial x} + \alpha_n\eta_n\frac{\partial\eta_n}{\partial x} + \beta_n\frac{\partial^3\eta_n}{\partial x^3} = 0, \tag{2}$$

where α_n is the nonlinearity coefficient, and β_n is the dispersion coefficient for the nth mode. Both coefficients are also called "environmental parameters" as they account for conditions such as stratification and water depth [*Lee and Beardsley*, 1974]

$$\alpha_n = \frac{3c_n}{2}\frac{\int_{-H}^{0}\left(\frac{dW_n(z)}{dz}\right)^3 dz}{\int_{-H}^{0}\left(\frac{dW_n(z)}{dz}\right)^2 dz} \tag{3}$$

$$\beta_n = \frac{c_n}{2}\frac{\int_{-H}^{0}W(z)_n^2 dz}{\int_{-H}^{0}\left(\frac{dW_n(z)}{dz}\right)^2 dz}. \tag{4}$$

An analytical solution of the K-dV equation is the following squared hyperbolic secant function: $\eta_n(x, z, t) =$

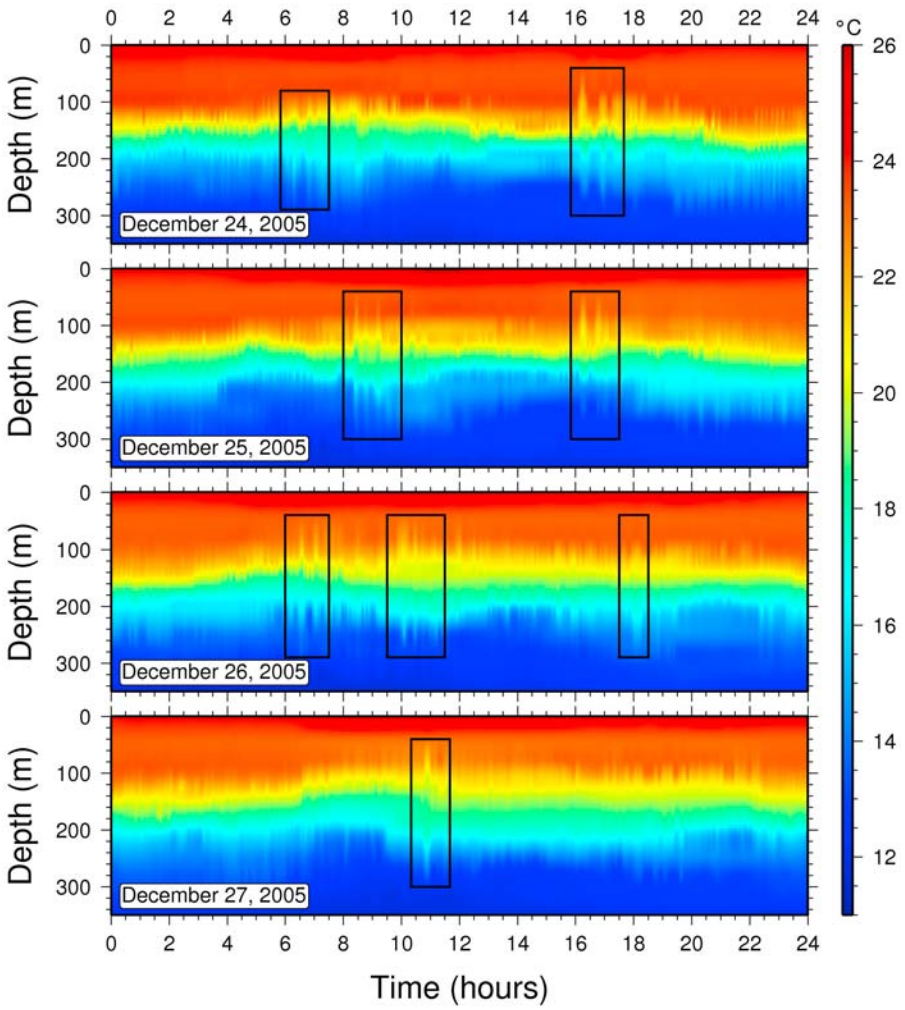

Figure 5. Same as Figure 3 except during winter (24–27 December 2005).

$\eta_{0,n}W_n(z)\mathrm{sech}^2((x - C_n t/\Delta_n))$, where $\eta_{0,n}$ is the amplitude, $C_n = c_n + (\alpha_n\eta_{0,n}/3)$ is the nonlinear phase speed, and $\Delta_n = \sqrt{12\beta_n/\alpha_n\eta_{0,n}}$ is the nonlinear characteristic width. The wave width (Δ_n) and amplitude ($\eta_{0,n}$) are inversely related such that narrow waves have larger amplitude and nonlinear phase speed (C_n) accordingly [*Apel et al.*, 1997].

3.1.2. Vertical Structures

[17] The vertical velocity component, w, was estimated from the temperature measurements using the temperature conservation equation based on the assumption of negligible nonlinear and horizontal advection [*Apel et al.*, 1997]

$$w(z,t) \approx -\frac{\dfrac{T^h(z,t) - T^h(z,t-\Delta t)}{\Delta t}}{\dfrac{T^b(z+\Delta z,t) - T^b(z,t)}{\Delta z}}, \qquad (5)$$

where $T^h(z, t)$ is the 5 hour high-pass-filtered temperature, $T^b(z, t)$ is the 36 hour low-pass-filtered temperature, z is the depth where the temperature sensor was mounted, Δz is the depth difference between the two temperature sensors, t is the time when the mode 2 ISW passed the mooring, and Δt is 1 min.

[18] Since most of the mode 2 ISWs were propagating to the west (see Figures 4 and 7), and the horizontal velocity profile induced by an ISW is parallel to its propagating direction, here we display only the fluctuations of the eastward current component (u'), after removing the background current. Figures 8a and 8c display the mode 2 ISW vertical structure function of horizontal motion $U_2(z)$ and the vertical profile of $u'(z)$ at 2340 UT on 27 June 2005 and at 1052 UT on 27 December 2005, respectively. Figures 8b and 8d show the mode 2 ISW vertical structure function of vertical motion $W_2(z)$ and the vertical profile of the vertical current component $w(z)$ at 2332 UT on 27 June 2005 and at 1044 UT on 27 December 2005, respectively. In general, the linear theory results of $U_2(z)$ and $W_2(z)$ agree well with the measurement results of $u(z)$ and $w(z)$, respectively. According to the vertical profile of $w(z)$, the nodal point of vertical velocity was located at approximately 110 m, while $W_2(z)$ indicated that the nodal point of vertical velocity was near 90 m depth. In the vertical profile of $u(z)$, two nodal points of horizontal velocity were located close to depths of 70 and 210 m, and $U_2(z)$ showed zero crossings of horizontal

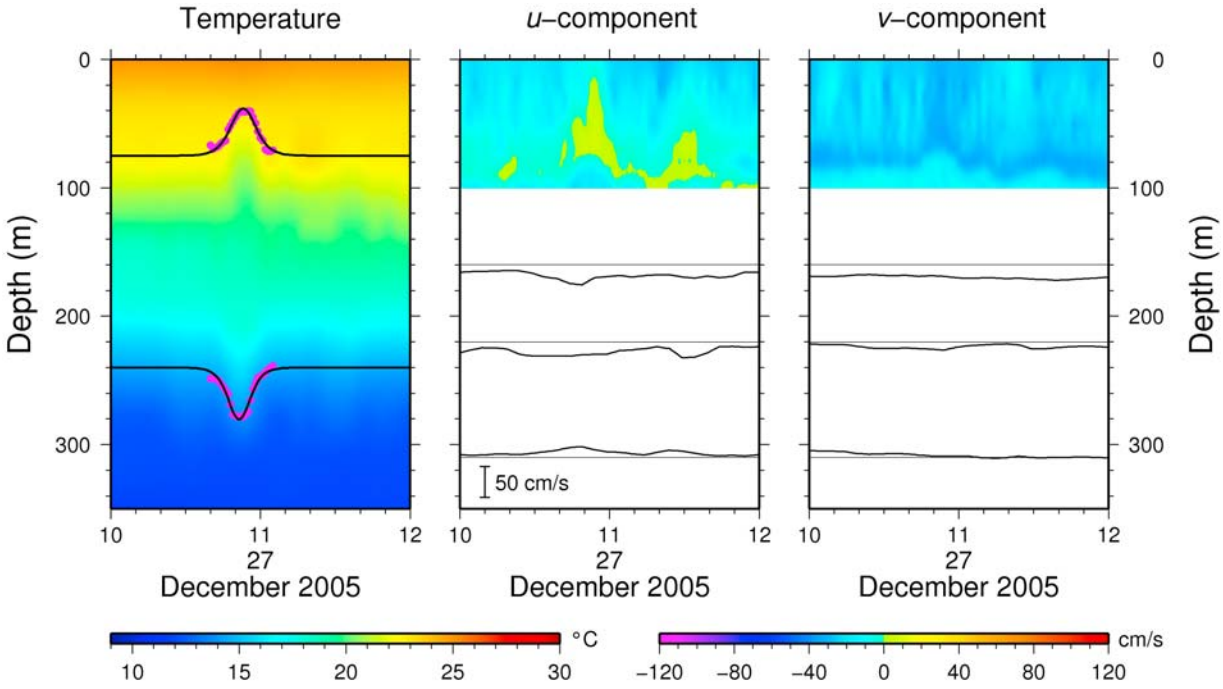

Figure 6. Same as Figure 2 except from 1000 to 1200 UT on 27 December 2005.

velocity around depths of 50 and 220 m. The vertical structures of the observations and linear model estimates generally agree well. The analysis also indicates that the vertical structure of these mode 2 ISWs can be well approximated by the linear theory for these observations.

3.1.3. Environmental Parameters of the K-dV Equation

[19] From the structure functions estimated above, the linear phase speeds (c_2), nonlinearity coefficients (α_2), and dispersion coefficients (β_2) of mode 2 ISWs were obtained. These results are shown in Table 3. Combining those results in summer and winter, the environmental coefficients of mode 2 ISWs were of the same order as those of mode 1 ISWs, whereas the linear phase speeds of mode 2 ISWs were slower than those of mode 1 ISWs [*Liu et al.*, 2004]. The notable finding is that the nonlinearity coefficients, α_2, in winter were larger than those in summer by a factor of 3. This result indicates significant seasonal variation of the thermal structure in this area, as discussed later.

3.1.4. Amplitudes and Characteristic Scales

[20] We identified 20 mode 2 ISWs in summer and 58 in winter. Most of the mode 2 ISW episodes had maximum temperature fluctuation around 75 and 240 m, with vertical structures similar to those shown in Figure 8. The two nodal points of horizontal velocity were most commonly found near 75 and 240 m. Accordingly, the isothermal variations at 75 and 240 m when a mode 2 ISW passed were used to represent the amplitude in the upper and lower water column, respectively. The isopycnal displacement induced by the mode 2 ISW was calculated by integrating equation (5). Alternatively, the evolution of the mode 2 ISW-induced isopycnal displacement can be described by the K-dV solution written as $\eta(z, t) \approx \widetilde{\eta}_0(z)\mathrm{sech}^2(t/\tau)$, where $\widetilde{\eta}_0(z)$ is the amplitude of the mode 2 ISW at z, and τ is the characteristic time scale. The 5 hour high-pass-filtered η at 75 and 240 m was fit to the sech^2 function. Only the isopycnal variation at 240 m was used to estimate τ. Figures 2 (left) and 6 (left) show the wave-induced isopycnal displacements (solid circles) at 75 and 240 m and the sech^2 profiles (bold lines) for the summer and winter cases, respectively. These results show that, for the present observations, the isopycnal temporal evolution of the mode 2 ISW was well described by the weakly nonlinear K-dV theory.

[21] A thermal displacement was only considered to be a wave when the amplitudes at both 75 and 240 m were

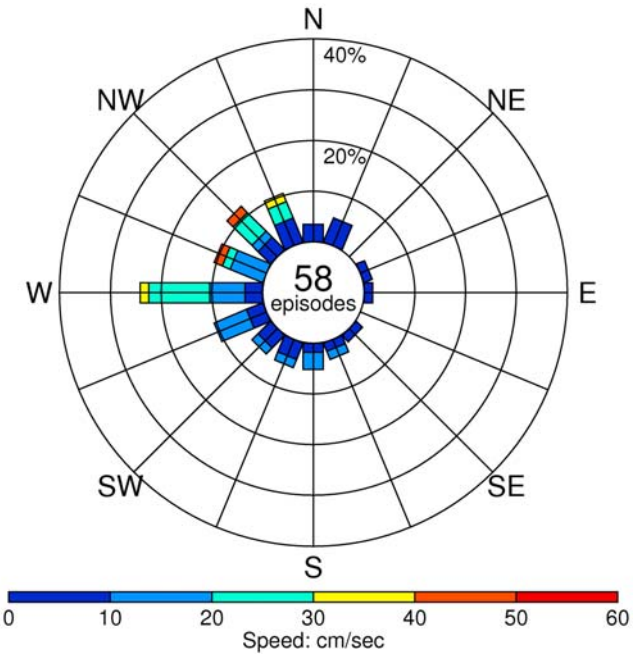

Figure 7. Same as Figure 4 except in winter.

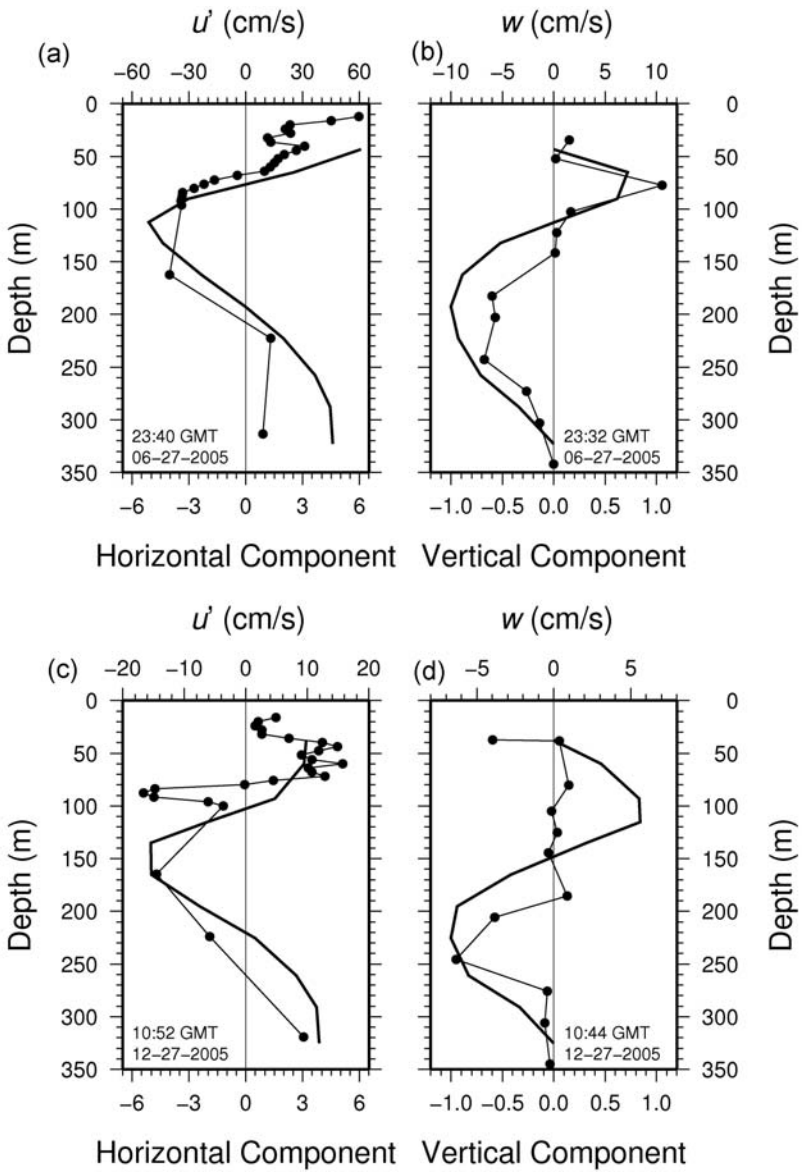

Figure 8. A comparison of the observed ($u'(z)$, $w(z)$) and calculated ($U_2(z)$, $W_2(z)$) vertical structure for the (a and b) summer and (c and d) winter time periods. The thin solid line indicates the observations and the thick solid line the calculation. Figures 8a and 8c compare the u components and Figures 8b and 8d compare the w components. The u and w are offset in time, with u corresponding to the time the wave passed, and w corresponding to 8 min before. All data were high-pass filtered to remove the background currents.

greater than 10 m. Similarly, the average characteristic time scale was included only if the corresponding wave amplitude was above the 10 m threshold. Table 3 shows the calculated isopycnal amplitudes and characteristic time scales. In summer, the average amplitude was 20 ± 14 m at 75 m and −22 ± 15 m at 240 m. The average characteristic time scale was 8.0 ± 4.3 min. In winter, the average amplitude was 30 ± 18 m at 75 m and −26 ± 16 m at 240 m. The average characteristic time scale was 6.9 ± 4.6 min. Mode 2 ISWs thus had larger amplitudes and smaller time scales in winter. The observed characteristic time scales were close to the K-dV model results (given in Table 3). Again, the vertical structure of mode 2 ISWs could be described by the linear theory modal function for these observations.

3.2. Relationship Between Mode 2 ISWs and Tides

[22] *Yang et al.* [2004] noted that the appearance (disappearance) of mode 1 ISWs coincided mostly with the spring (neap) tide, with few cases seen during the neap tide period. In this study, we performed a similar analysis for mode 2 ISWs. Figure 9 shows the percentage of total occurrence of mode 2 ISWs on each date relative to the full or new moon in summer and winter. In general, −3 to +3 days represents the spring tide period and the other days represent the neap tide period. In summer, 65% of mode 2 ISWs appeared during the spring tide, whereas 35% occurred during the neap tide. Most of the mode 2 ISWs (90%) appeared 12 hours after mode 1 ISWs. In winter, 34.5% of mode 2 ISWs appeared during the spring tide, whereas 65.5% occurred

Table 3. Comparison of the Weakly Nonlinear K-dV Model Results and Observations for Second Baroclinic Mode Internal Solitary Waves in Summer and Winter

	K-dV Model		Observation	
	Summer	Winter	Summer	Winter
α_2 ($\times 10^{-3}$ Hz)	2.01 ± 0.41	6.43 ± 1.02	–	–
β_2 ($\times 10^3$ m^3/s)	2.95 ± 0.13	1.21 ± 0.12	–	–
c_2 (m/s)	0.45 ± 0.01	0.35 ± 0.01	–	–
$\widetilde{\eta}_0$ (75)	–	–	20 ± 14	30 ± 18
$\widetilde{\eta}_0$ (240)	–	–	−22 ± 15	−26 ± 16
$\eta_{0,2}$	38.7 ± 26.1[a]	36.0 ± 16.2[a]	–	–
Δ_2 (m)	805 ± 297	274 ± 77	–	–
C_2 (m/s)	0.47 ± 0.02	0.43 ± 0.03	–	–
τ_2 (min)	14.3 ± 5.7[b]	5.4 ± 1.9[b]	8.0 ± 4.3	6.9 ± 4.6

[a]Calculated by $\widetilde{\eta}_0(75)/W_2(75)$ and $\widetilde{\eta}_0(240)/W_2(240)$.
[b]Calculated by Δ_2/C_2.

during the neap tide. Only 28% of mode 2 ISWs appeared after mode 1 ISWs during spring tide.

[23] The moored data indicate that mode 2 ISWs appeared following mode 1 ISWs during the spring tide in summer. This phenomenon can be also seen on satellite images. Figure 10 is a Moderate Resolution Imaging Spectroradiometer (MODIS) image captured at 0310 UT on 21 May 2001 (spring tide). Signals revealed two ISW packets with "dark-bright" bands northeast and northwest of Dongsha Atoll. According to the curvature of the leading wave and subsequent waves, these two wave packets were primarily propagating westward. However, it is difficult to identify the polarity of a mode 1 ISW using an optical satellite image because the color of the wave crest of an ISW is not only a function of sea surface roughness (or the convergence/divergence area) induced by an ISW [*Alpers*, 1985; *Liu et al.*, 1998] but is also related to the sun elevation and satellite viewing angles [*Mitnik et al.*, 2000]. However, the eastern-most two wave packets with dark-bright bands were likely mode 1 depression waves because the local water depths were still deep [*Yang et al.*, 2004; *Ramp et al.*, 2004]. Interestingly, there are signs that two waves with "bright-dark" bands were present in between two wave packets with dark-bright bands (or two mode 1 depression ISWs) in the vicinity of 21°10′N, 117°10′E and 21°38′N, 117°15′E. The bright-dark wave crest could be considered to be a mode 1 elevation wave. However, an elevation wave cannot exist if the local water is deep. In theoretical considerations, the pattern of the upper part of a mode 2 ISW is the same as that of a mode 1 elevated wave. Accordingly, the bright-dark wave crests could indicate that a mode 2 ISW packet was present, propagating westward. This MODIS image result agreed with the moored observations showing that mode 2 ISWs appeared in between two mode 1 depression ISWs during the spring tide period.

[24] In the neap tide period during summer, several mode 1 ISWs were observed, and mode 2 ISWs appeared occasionally. Similar episodes occurred during the spring tide in winter, where mode 2 ISWs appeared following mode 1 ISWs. However, during the neap tide in winter, the observations showed the emergence of numerous mode 2 ISWs while mode 1 ISWs or internal tides could not be identified. The abundance of mode 2 ISWs during winter could be related to seasonal changes in the local stratification.

3.3. Seasonal Variation

3.3.1. Stratification

[25] Figure 11 shows contours of the buoyancy frequency N in summer and winter. The thermocline was located at around 80 ∼ 100 m and 150 ∼ 200 m in summer and winter, respectively. Under the condition of a deeper thermocline, mode 2 ISWs seemed to emerge more frequently whereas mode 1 ISWs were rare. Consequently, a deeper thermocline is more favorable for mode 2 ISWs, as discussed in section 3.3.2.

3.3.2. Nonlinearity Coefficient

[26] Figures 3 and 5 show mode 1 ISWs occurred less frequently in winter than in summer. Figure 11 illustrates the significant changes in seasonal stratification. These changes indicate the variability of the nonlinearity coefficients α_1 and α_2 in the K-dV equation, which were used to estimated the seasonal differences of the internal wavefield. Figure 12 shows a comparison between the variations in α_1 and α_2 in summer and winter. Values of α_1 were always negative in summer and near zero in winter, and α_2 values in winter were always larger than those in summer. These results agree well with observations. Mode 1 ISWs appeared frequently in the form of depression waves (negative α_1) in summer. In winter, mode 1 ISWs also seemed to vanish as α_1 neared zero. Mode 2 ISWs appeared more frequently in winter (larger α_2) than in summer (smaller α_2).

4. Discussion and Summary

[27] Stratification had a significant effect on the emergence of mode 2 ISWs. Figure 13 shows two vertical profiles of density in summer and winter. Figure 13 (left)

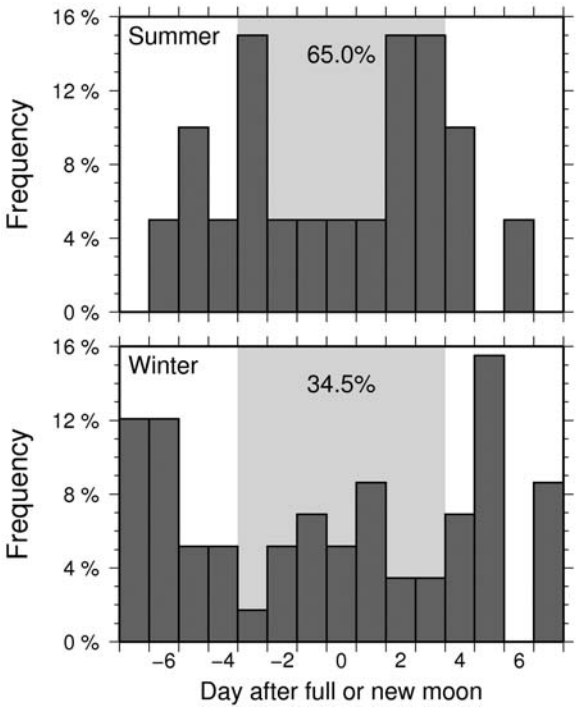

Figure 9. The percentage of total occurrence of mode 2 ISWs relative to the lunar cycle. Results are shown for (top) summer and (bottom) winter.

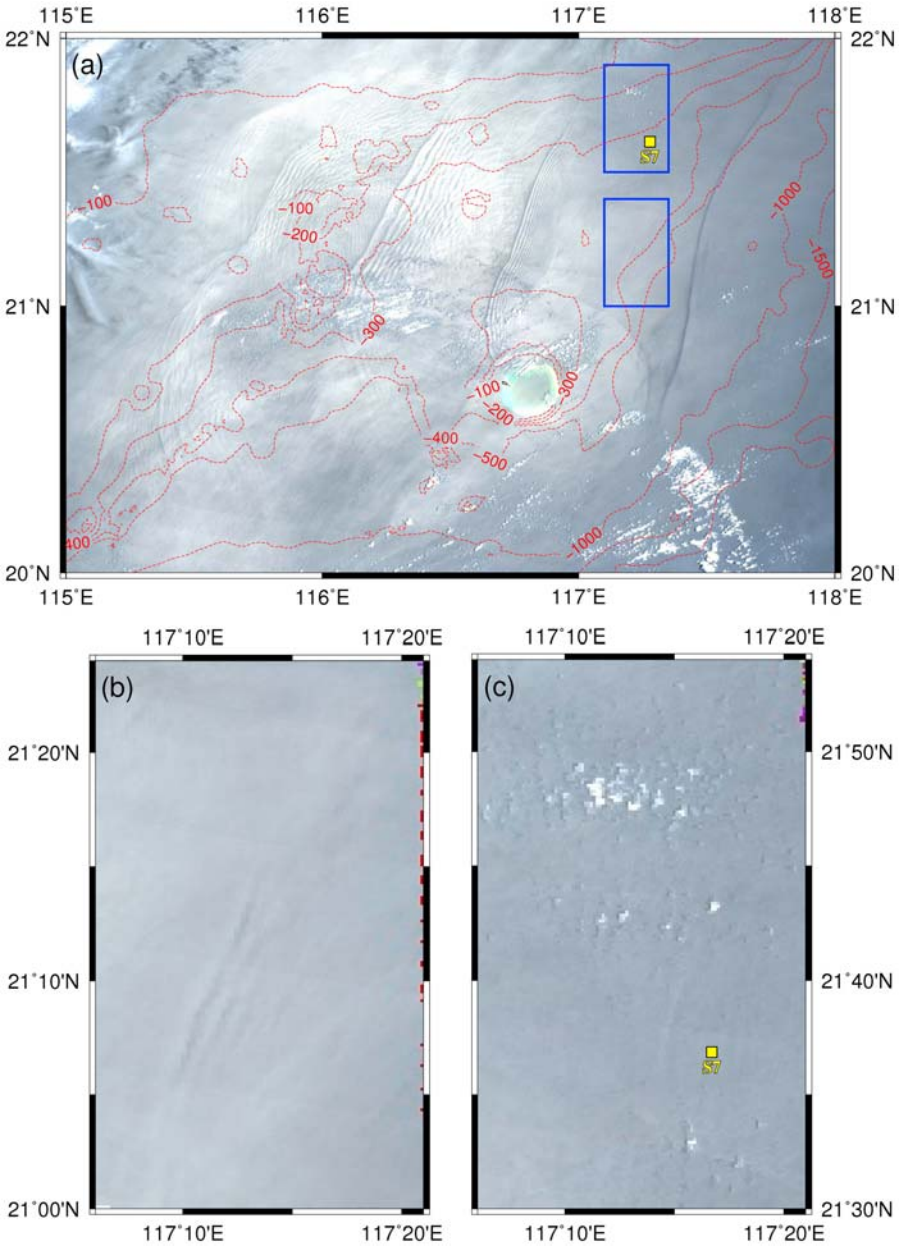

Figure 10. (a) MODIS (bands 1, 3, and 4) 250 m resolution visible image near Dongsha Atoll acquired on 21 May 2001 at 0310 UT. Enlarged images framed by the (b) lower and (c) upper blue rectangles are shown. The depth contours (red dashed lines) are shown at 200 m intervals between 100 and 500 m. The 1000 and 1500 m isobaths are also shown. The yellow solid square represents the mooring location.

shows the density profile at 2300 UT on 27 June 2005, and Figure 13 (right) shows the density profile at 1442 UT on 12 December 2005. To focus on the state that was not disturbed by the mode 2 ISW, both profiles were chosen for a time before the mode 2 ISW passed the mooring location. Figure 13 (left) shows that continuous stratification existed in summer. The stratification corresponded to a shallow thermocline. Under this stratification, mode 1 depression ISWs frequently occurred across the continental slope. In these observations, 90% of mode 2 ISWs in summer appeared after mode 1 ISWs. Hence, mode 2 ISWs may be related to the shoaling process of mode 1 ISWs or internal tides.

[28] Figure 13 (right) shows a different stratification in winter. The thermocline was located between 130 and 250 m. Two relatively uniform density layers existed above and below the thermocline. This thermal structure appeared as a thin layer bounded by two thick layers, approximating a hyperbolic tangent profile. Theoretical studies by *Benjamin* [1967] suggested that a mode 2 ISW could exist under a density structure with a hyperbolic tangent profile. Additionally, *Davis and Acrivos* [1967] generated a mode 2 ISW in a three-layer water tank under this density structure. Numerous other studies on mode 2 ISWs have also used hyperbolic tangent density profiles. Accordingly, the density structure could be a crucial factor for mode 2 ISWs.

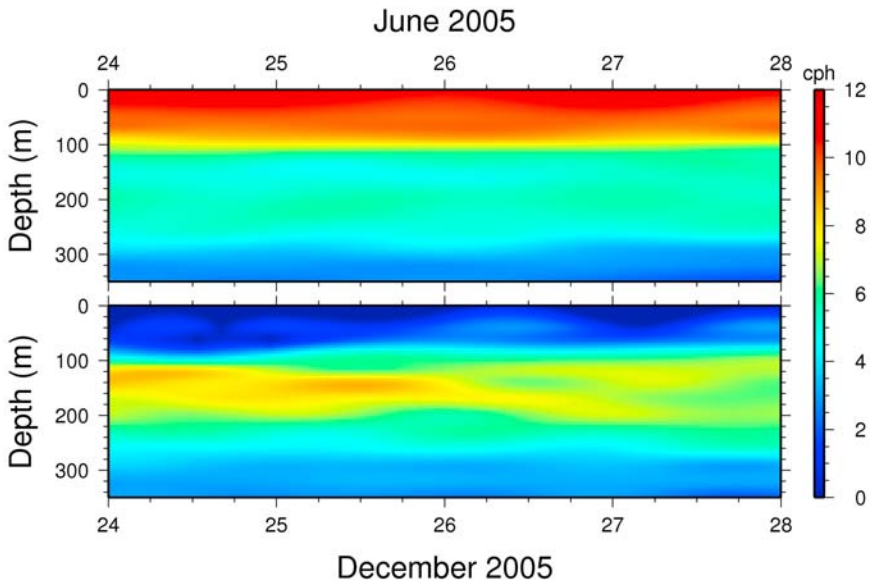

Figure 11. Contours of the buoyancy frequency (top) from 24 to 27 June 2005 and (bottom) from 24 to 27 December 2005.

Examining our observations, this density structure was often seen during the neap tide in winter.

[29] The relationship between the mode 1 and mode 2 ISWs during the spring tide in winter was similar to that during the spring tide in summer, but in winter only 28% of mode 2 ISWs appeared and followed mode 1 ISWs. However, there were many mode 2 ISWs during the neap tide in winter. In this stage, mode 1 ISWs became vague and the density structure was like a hyperbolic tangent profile. These mode 2 ISWs were not similar to those in summer; instead, they may have been related to the density structure. Evidence from late December 2005 and late February 2006 suggests that the thermocline was deep and a number of mode 2 ISWs were observed during these periods. Thus, these mode 2 ISWs had low correlation to the shoaling of the mode 1 ISWs or internal tides. A deeper thermocline could be favorable for mode 2 ISWs. The frequent emergence of mode 2 ISWs could be a local event under a condition of stratification with a thick surface mixed layer and a deeper thermocline.

[30] Table 4 indicates the nonlinearity and dispersion coefficients for the two vertical profiles of density in summer and winter shown in Figure 13. The seasonal difference is apparent; values of α_1 were nearly 31.6 times larger in summer than in winter. Consequently, α_2 was nearly 3.6 times larger in winter than in summer. In theoretical considerations, the nonlinearity coefficients (α_n) are very sensitive to stratification, whereas the dispersion coefficients

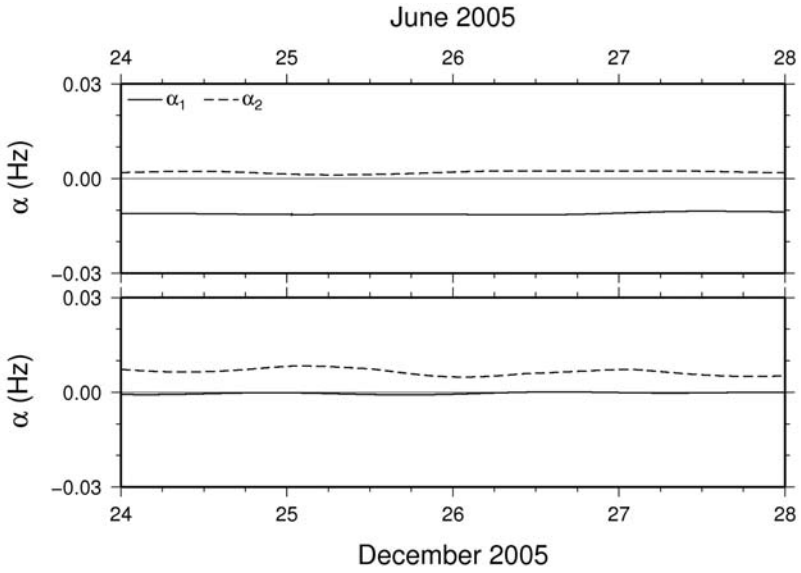

Figure 12. The first (α_1, solid line) and second (α_2, dashed line) mode nonlinearity coefficients of the K-dV equation (top) from 24 to 27 June 2005 and (bottom) from 24 to 27 December 2005.

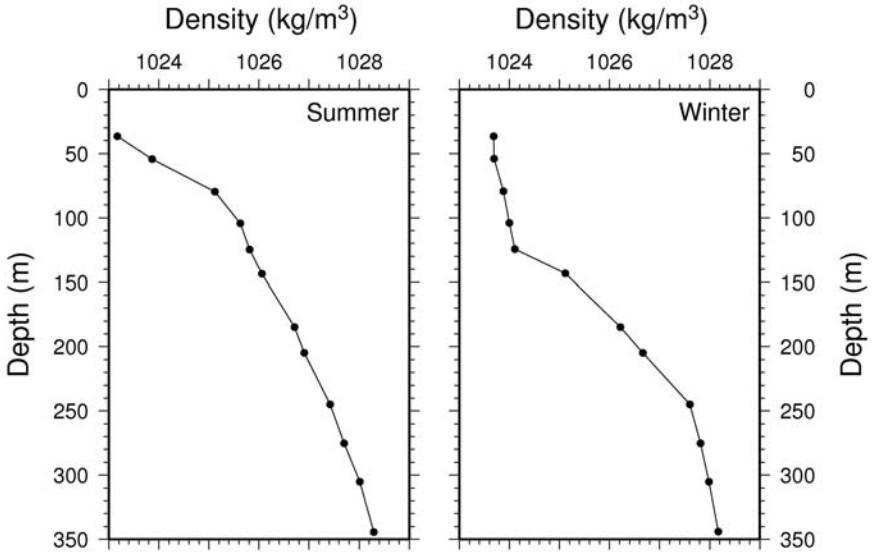

Figure 13. The density profile (left) at 2300 UT on 27 June 2005 and (right) at 1442 UT on 24 December 2005.

(β_n) are weakly dependent on the details of the stratification [*Holloway and Pelinovsky*, 2002]. The ratio between the nonlinearity coefficient and the dispersion coefficient, the Ursell number, affects the nature of the waveform. That is, a solitary waveform occurs when the Ursell number is large, and a linear sinusoidal waveform occurs when the Ursell number is small [*Lee and Beardsley*, 1974; *Holloway and Pelinovsky*, 2002]. Therefore, the seasonal change in stratification will affect the nature of the waveform. The Ursell number for mode 1 in winter was only 2% of that in summer. Nevertheless, the Ursell number for mode 2 in winter was nearly eight times greater than that in summer. These results indicate that it is difficult for mode 1 ISWs to evolve when there is a main pycnocline near the middepth in winter and that mode 2 ISWs develop more easily in winter than in summer.

[31] Using VANS/WISE mooring observations in the northern South China Sea, data collected by the thermistor chain and current meters revealed a number of mode 2 ISW signals. Typically, mode 2 ISWs show upward (downward) displacement in the upper (lower) water column, respectively. In summer, mode 2 ISWs may relate to the diurnal tide with a period of about 24 hours. In winter, mode 2 ISWs emerged randomly but frequently. According to previous studies, the modal displacement η_n and its vertical structure are well described by the weakly nonlinear K-dV theory. The amplitude and the characteristic time scale can be fit by a squared hyperbolic secant function. Accordingly in summer, mode 2 ISWs displaced isotherms by 20 ± 14 m at 75 m and -22 ± 15 m at 240 m. The characteristic time scale was about 8.0 ± 4.3 min. In winter, the average amplitude was 30 ± 18 m at 75 m and -26 ± 16 m at 240 m, and the average characteristic time scale was 6.9 ± 4.6 min. The mode 2 ISWs had larger amplitudes and smaller time scales in winter than in summer. Most mode 2 ISWs propagated westward. In summer, most mode 2 ISWs emerged during the spring tide period. In contrast, most mode 2 ISWs were found during the neap tide in winter. This seasonal difference could be associated with the thermal structure. The buoyancy frequency in summer and winter shows that the thermocline was deep in winter. When the thermocline was deep and reached near middepth, mode 2 ISWs were observed more frequently whereas mode 1 ISWs were vague. A deeper thermocline could be favorable for mode 2 ISWs.

[32] Stratification had a significant effect on the emergence of mode 2 ISWs. Continuous stratification existed in summer and corresponded to a shallow thermocline. The observations showed that most mode 2 ISWs followed mode 1 ISWs in summer. These results suggest that a mode 2 ISW may be related to the shoaling process of a mode 1 ISW or internal tide.

[33] In winter, numerous mode 2 ISWs were observed during the neap tide. Mode 1 ISWs became vague, and the vertical density structure resembled a hyperbolic tangent

Table 4. Comparison of the Nonlinearity and Dispersion Coefficients and the Ursell Numbers for First and Second Baroclinic Mode Internal Solitary Waves in Summer and Winter[a]

	Mode 1			Mode 2		
	α_1 ($\times 10^{-3}$ Hz)	β_1 ($\times 10^3$ m^3/s)	α_1/β_1 ($\times 10^{-6}$ m^{-3})	α_2 ($\times 10^{-3}$ Hz)	β_2 ($\times 10^3$ m^3/s)	α_2/β_2 ($\times 10^{-6}$ m^{-3})
Summer	−10.52	9.46	−1.112	1.86	2.91	0.640
Winter	−0.33	12.57	0.026	6.74	1.25	5.402

[a]Here α is the nonlinearity coefficient, β is the dispersion coefficient, and α/β is the Ursell number.

profile. These mode 2 ISWs were not similar to those in summer; instead, they may have been related to density structure. A density structure with a main pycnocline near the middepth could be favorable for the development of mode 2 ISWs.

[34] The Ursell number affects the nature of the waveform. A solitary waveform occurs when the Ursell number is large, while a more sinusoidal waveform occurs when the Ursell number is small. The Ursell number for mode 1 in winter was smaller, indicating that it is difficult for mode 1 ISWs to evolve when the main pycnocline is near middepth. Nevertheless, the Ursell number for mode 2 was larger in winter than in summer. Thus, mode 2 ISWs can develop more easily in winter than in summer. This result also confirms that stratification was the cause of the seasonal variation of mode 2 ISW occurrences. Further study is needed to elucidate the different mechanisms that generate mode 2 ISWs in summer and winter.

[35] **Acknowledgments.** This study was supported by the National Science Council, Taiwan, under grants NSC 93-2611-M-012-001 and NSC 94-2611-M-012-001 for Y.J.Y., NSC 94-2611-M-268-001 and NSC 95-2611-M-268-001 for C.C.K., and NSC 93-2611-M-002-019 and NSC 94-2611-M-002-003 for T.Y.T. and the Office of Naval Research, USA, for S.R.R. The authors would like thank the technical support groups at National Taiwan University and the Naval Postgraduate School, who all worked tirelessly to execute the fieldwork at sea. The assistance of the captain and crewmembers of the R/V *Ocean Researcher I* is greatly appreciated.

References

Akylas, T., and R. Grimshaw (1992), Solitary internal waves with oscillatory tails, *J. Fluid Mech.*, *242*, 279–298, doi:10.1017/S0022112092002374.

Alpers, W. (1985), Theory of radar imaging of internal waves, *Nature*, *314*, 245–247, doi:10.1038/314245a0.

Antenucci, J. P., J. Imberger, and A. Saggio (2000), Seasonal evolution of basin-scale internal wave field in a large stratified lake, *Limnol. Oceanogr.*, *45*, 1621–1638.

Apel, J. R. (2003), A new analytical model for internal solitons in the ocean, *J. Phys. Oceanogr.*, *33*, 2247–2269, doi:10.1175/1520-0485(2003)033<2247:ANAMFI>2.0.CO;2.

Apel, J. R., et al. (1997), An overview of the 1995 SWARM Shallow-Water Internal Wave Acoustic Scattering Experiment, *IEEE J. Oceanic Eng.*, *22*, 465–500, doi:10.1109/48.611138.

Apel, J. R., L. A. Ostrovsky, Y. A. Stepanyants, and J. F. Lynch (2007), Internal solitons in the ocean and their effect on underwater sound, *J. Acoust. Soc. Am.*, *121*, 695–722, doi:10.1121/1.2395914.

Benjamin, T. B. (1967), Internal waves of permanent form in fluids of great depth, *J. Fluid Mech.*, *29*, 559–592, doi:10.1017/S002211206700103X.

Boegman, L., and G. N. Ivey (2009), Flow separation and resuspension beneath shoaling nonlinear internal waves, *J. Geophys. Res.*, *114*, C02018, doi:10.1029/2007JC004411.

Boegman, L., J. Imberger, G. N. Ivey, and J. P. Antenucci (2003), High-frequency internal waves in large stratified lakes, *Limnol. Oceanogr.*, *48*, 895–919.

Bogucki, D. J., L. G. Redekopp, and J. Barth (2005), Internal solitary waves in the Coastal Mixing and Optics 1996 experiment: Multimodal structure and resuspension, *J. Geophys. Res.*, *110*, C02024, doi:10.1029/2003JC002253.

Bole, J. B., C. C. Ebbesmeyer, and R. D. Romea (1994), Soliton currents in the South China Sea: Measurements and theoretical modeling, paper presented at 26th Annual Offshore Technology Conference, Soc. of Pet. Eng., Houston, Tex.

Chao, S.-Y., P.-T. Shaw, M.-K. Hsu, and Y. J. Yang (2006), Reflection and diffraction of internal solitary waves by a circular island, *J. Oceanogr.*, *62*, 811–823, doi:10.1007/s10872-006-0100-4.

Chao, S.-Y., D.-S. Ko, R.-C. Lien, and P.-T. Shaw (2007), Assessing the west ridge of Luzon Strait as an internal wave mediator, *J. Oceanogr.*, *63*, 897–911, doi:10.1007/s10872-007-0076-8.

Davis, R. E., and A. Acrivos (1967), Solitary internal waves in deep water, *J. Fluid Mech.*, *29*, 593–607, doi:10.1017/S0022112067001041.

Duda, T. F., J. F. Lynch, J. D. Irish, R. C. Beardsley, S. R. Ramp, C.-S. Chiu, T. Y. Tang, and Y. J. Yang (2004), Internal tide and nonlinear internal wave behavior at the continental slope in the northern South China Sea, *IEEE J. Oceanic Eng.*, *29*, 1105–1130, doi:10.1109/JOE.2004.836998.

Farmer, D. M., and J. D. Smith (1980), Tidal interaction of stratified flow with a sill in Knight Inlet, *Deep Sea Res. Part A*, *27*, 239–254, doi:10.1016/0198-0149(80)90015-1.

Gill, A. E. (1982), *Atmosphere-Ocean Dynamics*, 662 pp., Academic, San Diego, Calif.

Helfrich, K. R., and R. H. J. Grimshaw (2008), Nonlinear disintegration of the internal tide, *J. Phys. Oceanogr.*, *38*, 686–701, doi:10.1175/2007JPO3826.1.

Helfrich, K. R., and W. K. Melville (1986), On long nonlinear internal waves over slope-shelf topography, *J. Fluid Mech.*, *167*, 285–308, doi:10.1017/S0022112086002823.

Helfrich, K. R., and W. K. Melville (2006), Long nonlinear internal waves, *Annu. Rev. Fluid Mech.*, *38*, 395–425, doi:10.1146/annurev.fluid.38.050304.092129.

Holloway, P., and E. Pelinovsky (2002), Internal tide transformation and oceanic internal solitary waves, in *Environmental Stratified Flows*, edited by R. Grimshaw, pp. 29–60, Kluwer Acad., Boston.

Honji, H., N. Matsunaga, Y. Sugihara, and K. Sakai (1995), Experimental observation of internal symmetric solitary waves in a two-layer fluid, *Fluid Dyn. Res.*, *15*, 89–102, doi:10.1016/0169-5983(94)00032-U.

Kao, C.-C., M.-J. Huang, and Y. J. Yang (2006), Feature extraction of oceanic internal wave base on remote sensing imagery, paper presented at Management Association for Private Photogrammetric Surveyors 2006 Fall Conference, Am. Soc. for Photogramm. and Remote Sens., San Antonio, Tex.

Kao, C.-C., L.-H. Lee, C.-C. Tai, and Y.-C. Wei (2007), Extracting the ocean surface feature on non-linear internal solitary waves in MODIS satellite images, paper presented at Third International Conferences on Intelligent Information Hiding and Multimedia Signal Processing, Inst. of Electr. and Electr. Eng., Kaohsiung, Taiwan.

Kao, T. W., and H.-P. Pao (1980), Wake collapse in the thermocline and internal solitary waves, *J. Fluid Mech.*, *97*, 115–127, doi:10.1017/S0022112080002455.

Konyaev, K. V., K. D. Sabinin, and A. N. Serebryany (1995), Large-amplitude internal waves at the Mascarene Ridge in the Indian Ocean, *Deep Sea Res. Part I*, *42*, 2075–2091, doi:10.1016/0967-0637(95)00067-4.

Korteweg, D. J., and G. deVries (1895), On the change of the form of long waves advancing in a rectangular canal and on a new type of long stationary waves, *Philos. Mag.*, *39*, 422–443.

Lee, C.-Y., and R. C. Beardsley (1974), The generation of long nonlinear internal waves in a weakly stratified shear flow, *J. Geophys. Res.*, *79*, 453–462, doi:10.1029/JC079i003p00453.

Lien, R.-C., T. Y. Tang, M.-H. Chang, and E. A. D'Asaro (2005), Energy of nonlinear internal waves in the South China Sea, *Geophys. Res. Lett.*, *32*, L05615, doi:10.1029/2004GL022012.

Liu, A. K., Y. S. Chang, M.-K. Hsu, and N. K. Liang (1998), Evolution of nonlinear internal waves in the East and South China seas, *J. Geophys. Res.*, *103*, 7995–8008, doi:10.1029/97JC01918.

Liu, A. K., S. R. Ramp, Y. Zhao, and T. Y. Tang (2004), A case study of internal solitary wave propagation during the ASIAEX 2001, *IEEE J. Oceanic Eng.*, *29*, 1144–1156, doi:10.1109/JOE.2004.841392.

Lynch, J. F., S. R. Ramp, C.-S. Chiu, T. Y. Tang, Y. J. Yang, and J. A. Simmen (2004), Research highlights from the Asian Seas International Acoustics Experiment in the South China Sea, *IEEE J. Oceanic Eng.*, *29*, 1067–1074, doi:10.1109/JOE.2005.843162.

Maxworthy, T. (1980), On the formation of nonlinear internal waves from the gravitational collapse of mixed regions in two and three dimensions, *J. Fluid Mech.*, *96*, 47–64, doi:10.1017/S0022112080002017.

Mehta, A. P., B. R. Sutherland, and P. J. Kyba (2002), Interfacial gravity currents. Part II. Wave excitation, *Phys. Fluids*, *14*, 3558–3569, doi:10.1063/1.1503355.

Mitnik, L., W. Alpers, K. S. Chen, and A. J. Chen (2000), Manifestation of internal solitary waves on ERS SAR and SPOT images: Similarties and differences, paper presented at 2000 International Geoscience and Remote Sensing Symposium (IGARSS'00), Inst. of Electr. and Electr. Eng., Honolulu.

Moum, J. N., J. D. Nash, and J. M. Klymak (2008), Small-scale processes in the coastal ocean, *Oceanography*, *21*, 22–33.

Ramp, S. R., J. F. Lynch, P. H. Dahl, C.-S. Chiu, and J. A. Simmen (2003), Program fosters advances in shallow-water acoustics southeastern Asia, *Eos Trans. AGU*, *84*(37), 361, doi:10.1029/2003EO370001.

Ramp, S. R., T. Y. Tang, T. F. Duda, J. F. Lynch, A. K. Liu, C.-S. Chiu, F. L. Bahr, H.-R. Kim, and Y. J. Yang (2004), Internal solitons in the northeastern South China Sea. Part I: Sources and deep water propagation, *IEEE J. Oceanic Eng.*, *29*, 1157–1181, doi:10.1109/JOE.2004.840839.

Rubino, A., P. Brandt, and R. Weigle (2001), On the dynamics of internal waves in a nonlinear, weakly nonhydrostatic three-layer ocean, *J. Geophys. Res.*, *106*, 26,899–26,915, doi:10.1029/2001JC000958.

Rusås, P.-O., and J. Grue (2002), Solitary waves and conjugate flows in a three-layer fluid, *Eur. J. Mech. Part B*, *21*, 185–206, doi:10.1016/S0997-7546(01)01163-3.

Sabinin, K., and A. Serebryany (2005), Intense short-period internal waves in the ocean, *J. Mar. Res.*, *63*, 227–261, doi:10.1357/0022240053693879.

Saggio, A., and J. Imberger (1998), Internal wave weather in a stratified lake, *Limnol. Oceanogr.*, *43*, 1780–1798.

Saggio, A., and J. Imberger (2001), Mixing and turbulent fluxes in a metalimnion of a stratified lake, *Limnol. Oceanogr.*, *46*, 392–409.

Sandstrom, H., and J. A. Elliott (1984), Internal tides and solitons on the Scotian Shelf: A nutrient pump at work, *J. Geophys. Res.*, *89*, 6415–6426, doi:10.1029/JC089iC04p06415.

Shaw, P.-T., D. S. Ko, and S.-Y. Chao (2009), Internal solitary waves induced by flow over a ridge: With applications to northern South China Sea, *J. Geophys. Res.*, *114*, C02019, doi:10.1029/2008JC005007.

Stamp, A. P., and M. Jacka (1995), Deep-water internal solitary waves, *J. Fluid Mech.*, *305*, 347–371, doi:10.1017/S0022112095004654.

Stastna, M., and K. G. Lamp (2008), Sediment resuspension mechanisms associated with internal waves in coastal waters, *J. Geophys. Res.*, *113*, C10016, doi:10.1029/2007JC004711.

Stastna, M., and W. Peltier (2005), On the resonant generation of large-amplitude internal solitary waves and solitary-like waves, *J. Fluid Mech.*, *543*, 267–292, doi:10.1017/S002211200500652X.

Sutherland, B. R. (2002), Interfacial gravity currents. Part I. Mixing and entrainment, *Phys. Fluids*, *14*, 2244–2254, doi:10.1063/1.1483303.

Terez, D. E., and O. M. Knio (1998), Numerical simulations of large-amplitude internal solitary waves, *J. Fluid Mech.*, *362*, 53–82, doi:10.1017/S0022112098008799.

Tung, K.-K., T. F. Chan, and T. Kubota (1982), Large amplitude internal waves of permanent form, *Stud. Appl. Math.*, *66*, 1–44.

Vlasenko, V. I. (1994), Multimodal soliton of internal waves, *Atmos. Oceanic Phys.*, *30*, 161–169.

Vlasenko, V. I., and W. Alpers (2005), Generation of secondary internal waves by the interaction of an internal solitary wave with an underwater bank, *J. Geophys. Res.*, *110*, C02019, doi:10.1029/2004JC002467.

Vlasenko, V. I., and K. Hutter (2001), Generation of second mode solitary waves by the interaction of a first mode soliton with a sill, *Nonlinear Process. Geophys.*, *8*, 223–239.

Yang, Y. J., W.-D. Liang, T. Y. Tang, M.-K. Hsu, A. K. Liu, and M.-H. Chang (2000), ASIAEX 2000 South China Sea mooring data report, report, 67 pp., Natl. Taiwan Univ., Taipei.

Yang, Y. J., T. Y. Tang, M.-H. Chang, A. K. Liu, M.-K. Hsu, and S. R. Ramp (2004), Solitons northeast of Dongsha Island during the ASIAEX pilot studies, *IEEE J. Oceanic Eng.*, *29*, 1182–1199, doi:10.1109/JOE.2004.841424.

M.-H. Chang, Department of Marine Environmental Informatics, National Taiwan Ocean University, 2 Pei-Ning Road, Keelung 202, Taiwan. (mhchang@ntou.edu.tw)

Y. C. Fang and T. Y. Tang, Institute of Oceanography, National Taiwan University, Section 4, 1 Roosevelt Road, Taipei 106, Taiwan. (r94241103@ntu.edu.tw; tyt@ntu.edu.tw)

C.-C. Kao, Department of Information Management, Fortune Institute of Technology, 1-10 Nwongchang Road, Kaohsiung 831, Taiwan. (kcc7879@center.fotech.edu.tw)

S. R. Ramp, Monterey Bay Aquarium Research Institute, 7700 Sandholdt Road, Moss Landing, CA 95039, USA. (sramp@mbari.org)

Y. J. Yang, Department of Marine Science, Naval Academy, P.O. Box 90175, Kaohsiung 813, Taiwan. (yjyang@cna.edu.tw)